Geophysical Research Letters

RESEARCH LETTER
10.1029/2025GL117576

Moderate Thermal Conductivity of Fe-Ni-Si Alloy at Earth's Core Conditions: Implications for Core Thermal Evolution and Geodynamo

Wen-Pin Hsieh[1,2], Yi-Ting Chiang[1,2,3], Frédéric Deschamps[1], Chao-Chih Chen[1], Jen-Wei Chang[1], Daijo Ikuta[4], and Eiji Ohtani[5]

[1]Institute of Earth Sciences, Academia Sinica, Taipei, Taiwan, [2]Department of Geosciences, National Taiwan University, Taipei, Taiwan, [3]Department of Physics, National Taiwan University, Taipei, Taiwan, [4]Institute for Planetary Materials, Okayama University, Misasa, Japan, [5]Department of Earth Science, Tohoku University, Sendai, Japan

Abstract Earth's presently-active magnetic field is thought to be generated by geodynamo via convection of liquid outer core, primarily composed of Fe alloyed with Ni and light elements, for example, Si. Core thermal conductivity critically controls its thermal evolution, dynamics, and available energy (thermal vs. compositional) powering the geodynamo over Earth's history. Here we precisely measured thermal conductivity of solid $Fe_{0.85}Ni_{0.06}Si_{0.09}$ (Fe–7wt%Ni–5wt%Si) to 148 GPa/2950 K and Fe to 155 GPa/3246 K, respectively. We show that a liquid outer core with $Fe_{0.85}Ni_{0.06}Si_{0.09}$ has a moderate thermal conductivity of ~73 W m^{-1} K^{-1}, in the moderate zone over the previously reported broad range (~20–250 W m^{-1} K^{-1}) that includes various core compositions. Such a modest isentropic, conductive heat flow at core-mantle boundary (CMB) (~11 TW) is smaller than present-day CMB heat flow (~15 TW), suggesting a presently-active thermally-driven geodynamo and a maximum inner core age of ~0.8–1.3 billion-years.

Plain Language Summary Earth's stable, global magnetic field prevents our planet from being damaged by solar winds, a key feature for habitability compared to other terrestrial planets. The magnetic field is generated by vigorous convection of fluid outer core that requires sufficient energy (e.g., thermal and compositional convection) to operate. Core thermal conductivity plays a key role in determining the availability and temporal evolution of these energy sources. We here experimentally pin down the thermal conductivity of solid $Fe_{0.85}Ni_{0.06}Si_{0.09}$ (Fe–7wt%Ni–5wt%Si), a representative core composition, to ~86 W m^{-1} K^{-1} at 148 GPa and 2950 K. This suggests that the fluid outer core would have a moderate thermal conductivity of ~73 W m^{-1} K^{-1} at its topmost region. The modest cooling implies a minimum heat flow of ~11 TW required to sustain thermally-driven geodynamo. Given the present-day heat flow across core-mantle boundary of ~15 TW, our findings suggest that both thermal and compositional convection contribute to Earth's presently-active magnetic field. The inner core could be as old as ~0.8–1.3 billion-years, comparable to the timing inferred from increases in paleomagnetic field intensity.

Key Points:

- We measured thermal conductivity of solid $Fe_{0.85}Ni_{0.06}Si_{0.09}$ (Fe–7wt%Ni–5wt%Si) at high pressures and temperatures close to Earth's core
- A liquid outer core with $Fe_{0.85}Ni_{0.06}Si_{0.09}$ composition has a moderate thermal conductivity of ~73 W m^{-1} K^{-1} at its topmost region
- The moderate core thermal conductivity suggests a long-lived thermal dynamo and a modest maximum age, ~1 billion years, for inner core

Supporting Information:

Supporting Information may be found in the online version of this article.

Correspondence to:

W.-P. Hsieh,
wphsieh@earth.sinica.edu.tw

Citation:

Hsieh, W.-P., Chiang, Y.-T., Deschamps, F., Chen, C.-C., Chang, J.-W., Ikuta, D., & Ohtani, E. (2025). Moderate thermal conductivity of Fe-Ni-Si alloy at earth's core conditions: Implications for core thermal evolution and geodynamo. *Geophysical Research Letters*, *52*, e2025GL117576. https://doi.org/10.1029/2025GL117576

Received 12 JUN 2025
Accepted 24 OCT 2025

Author Contributions:

Conceptualization: Wen-Pin Hsieh, Eiji Ohtani
Formal analysis: Wen-Pin Hsieh, Yi-Ting Chiang, Daijo Ikuta, Eiji Ohtani
Funding acquisition: Wen-Pin Hsieh, Daijo Ikuta, Eiji Ohtani
Investigation: Wen-Pin Hsieh, Yi-Ting Chiang, Frédéric Deschamps, Chao-Chih Chen, Jen-Wei Chang, Daijo Ikuta, Eiji Ohtani
Methodology: Wen-Pin Hsieh
Project administration: Wen-Pin Hsieh

1. Introduction

Efficiencies of heat transport by conduction and convection through Earth's core and into the mantle fundamentally control our planet's thermochemical and magnetic evolutions, including the core cooling rate, dynamics, and available thermal and compositional energies powering convection-driven geodynamo for magnetic field (Hirose et al., 2013; Landeau et al., 2022; Q. Williams, 2018). To sustain a convective geodynamo with energy and entropy balances, sufficient thermal and/or compositional energies are required (Cormier et al., 2021; Labrosse, 2003, 2015; Landeau et al., 2022; Lay et al., 2008). Specifically, a pure thermally-driven geodynamo can be operated if the core-mantle boundary (CMB) heat flow (Q_{CMB}) is larger than a minimum value—isentropic heat flow by conduction at CMB (Q_a), which is proportional to core thermal conductivity ($\wedge_{core}$) at CMB. In contrast, if core is highly thermally conductive with Q_a larger than Q_{CMB}, a geodynamo can remain active as compositional convection occurs. Such compositional convection can be driven by transport of released buoyant elements via inner core solidification, or by exsolution/precipitation of light oxides, for example, MgO or SiO_2, from liquid outer core to CMB region (Badro et al., 2016; Hirose et al., 2017; O'Rourke & Stevenson, 2016). This latter mechanism was proposed to drive Earth's ancient dynamo since ~3.4 billion-years ago (Ga) (Tarduno et al., 2010), before inner core solidification.

Resources: Wen-Pin Hsieh, Daijo Ikuta, Eiji Ohtani
Supervision: Wen-Pin Hsieh
Validation: Wen-Pin Hsieh, Frédéric Deschamps
Writing – original draft: Wen-Pin Hsieh, Frédéric Deschamps
Writing – review & editing: Wen-Pin Hsieh, Yi-Ting Chiang, Frédéric Deschamps, Chao-Chih Chen, Jen-Wei Chang, Daijo Ikuta, Eiji Ohtani

Integration of seismology, cosmochemistry, and mineral physics have conclusively indicated that Earth's core is primarily composed of iron (Fe) alloyed with nickel (Ni) along with certain amounts (∼few wt%) of light elements, essentially silicon (Si), oxygen (O), sulfur (S), carbon (C), and hydrogen (H) (Cormier et al., 2021; Hirose et al., 2013, 2021; Li & Fei, 2003). Though the exact core composition remains uncertain, based on seismic data, mineral physics studies on the density, sound velocity, phase stability, and solubility of Fe-Ni-light element alloys suggested that among the light elements, Si is a likely candidate with ∼4 wt% in liquid outer core (Cormier et al., 2021; Hirose et al., 2013, 2021; Li & Fei, 2003). As heat conduction within the core is decisive for its thermochemical evolution, precise determination of the thermal conductivity ($\wedge$) of Fe-Ni-Si alloys at relevant core high pressure (P)-temperature (T) conditions is critically needed. This enables better assessing the age and growth rate of inner core, available energy sources sustaining geodynamo, and evolution of geomagnetic fields.

In the past decade, $\wedge_{core}$ with various potential compositions at high P-T conditions have been extensively investigated. First-principles calculations have coherently indicated a highly thermally conductive core ($\wedge_{core}$ ∼ 90–300 W m^{-1} K^{-1}), for example, (de Koker et al., 2012; Kleinschmidt et al., 2023; Pourovskii et al., 2020; Pozzo et al., 2012, 2014; Xu et al., 2018), though (Pozzo et al., 2022) recently reported a modest $\wedge_{core}$ of ∼80 W m^{-1} K^{-1} at CMB. In addition, electrical resistivity measurements have also been extensively performed and then used to infer the $\wedge_{core}$ via Wiedemann-Franz (WF) law with ideal Lorenz number, for example, (Berrada & Secco, 2021; Gomi et al., 2013, 2016; Ohta et al., 2016; Seagle et al., 2013; Yin et al., 2024; Y. Zhang et al., 2020, 2022). Similarly, the inferred $\wedge_{core}$ typically ranges from ∼90 to ∼250 W m^{-1} K^{-1}. In contrast, direct thermal conductivity measurements have been rare due to experimental challenges. Hsieh et al. (2020) reported $\wedge_{core}$ ∼ 20 W m^{-1} K^{-1} based on $Fe_{0.85}Si_{0.15}$ alloy, Konôpková et al. (2016) showed $\wedge_{core}$ ∼ 25–35 W m^{-1} K^{-1} based on Fe-light elements, Saha et al. (2020) predicted $\wedge_{core}$ ∼ 40 W m^{-1} K^{-1} based on pure Fe, while Hasegawa et al. (2024) suggested $\wedge_{core}$ ∼ 184 W m^{-1} K^{-1} based on pure Fe. Obviously, previous studies on the $\wedge_{core}$ is yet to reach a consensus. The discrepancy among literature results could be due to the reliability of different experimental and computational methods, the validity of WF law with ideal Lorenz number when converting electrical resistivity into thermal conductivity, as well as the uncertain effects of different light elements and melting on the thermal conductivity. Note that a highly thermally conductive core with rapid cooling would imply a short-lived thermally-driven geodynamo, yet an inner core as young as few hundred million years old, leading to the new core paradox (Olson, 2013). To reconcile the observed temporal evolution of paleomagnetic intensity since Archean or even Hadean (Biggin et al., 2015; Bono et al., 2019; Tarduno et al., 2010, 2015), a very high initial CMB temperature (T_{CMB}) or an early geodynamo powered by compositional convection via exsolution of light oxides, as mentioned above, would be required.

In this work, we combined an ultrafast optical pump-probe method with laser-heated diamond anvil cells (LHDAC) to precisely measure the thermal conductivity of solid $Fe_{0.85}Ni_{0.06}Si_{0.09}$ (Fe–7wt%Ni–5wt%Si), a representative core composition, to 148 GPa/2950 K and Fe to 155 GPa/3246 K, respectively. Our results represent the first direct measurements that pin down the $\wedge$ of a solid Fe-Ni-Si alloy to ∼86 W m^{-1} K^{-1} at the outermost core conditions, suggesting, in turn, a moderate $\wedge$ (∼73 W m^{-1} K^{-1}) for liquid outer core. Such a modest cooling rate of core would allow a presently-active thermally-driven geodynamo, along with a maximum inner core age of ∼1 billion-years (Gyrs).

2. Materials and Methods

2.1. Starting Materials and Sample Preparation

Single-crystalline pure Fe were from the same batch of samples we previously studied (Hsieh et al., 2020) (from Princeton Scientific Corporation). Polycrystalline powder of $Fe_{0.85}Ni_{0.06}Si_{0.09}$ were from the same batch of samples in Ikuta et al. (2021). We determined their chemical composition to be Fe and $Fe_{0.85}Ni_{0.06}Si_{0.09}$, respectively, by electron probe micro-analyzer.

We started the sample preparation by first polishing each sample down to ∼10 μm thick and depositing an ∼90 nm-thick aluminum (Al) film on the sample. We then loaded the sample of interest, together with a few ruby spheres as pressure calibrants, into a symmetric piston-cylinder diamond anvil cell equipped with a pair of 200 μm or 150–300 μm beveled culets and a rhenium gasket. For high pressure and room temperature measurements, we used silicone oil (CAS No. 63148-62-9 from ACROS ORGANICS) as the pressure medium. For simultaneously high P-T LHDAC measurements to ∼3250 K, we used MgO nanopowder (CAS No. 1309-48-4 from Merck with a typical grain size ≤50 nm) as the pressure medium and thermal insulating layer. We measured the pressure within

the sample chamber at room temperature (cold pressure) based on ruby's R_1 fluorescence peak (Shen et al., 2020) with a typical uncertainty of <2%. At P > ~50 GPa, we also collected the Raman spectrum of diamond anvil (Akahama & Kawamura, 2004) as an alternative pressure calibrant, which is in line with the pressure characterized by ruby fluorescence with a typical difference <3–5 GPa.

The heating-induced thermal pressure alters the effective pressure applied to the sample. We didn't in situ characterize the thermal pressure in our LHDAC experiments. Nevertheless, the thermal pressure ΔP_{th} is approximated as $\alpha K \Delta T$, where α, K, and ΔT are the thermal expansion coefficient, bulk modulus, and temperature change of the heated material, respectively (J. S. Zhang et al., 2015). The ΔP_{th} is thus empirically estimated to be ~few to 10 GPa (~few % of the initial cold pressure) in our high P-T measurement range (Dobrosavljevic et al., 2022; Hasegawa et al., 2024; J. S. Zhang et al., 2015). Such heating-induced pressure uncertainty has been taken into account in our data analysis, see Section 2.2 below. Details of the experimental setup, sample geometry, collected thermal radiation spectra, and modeled temperature profile for LHDAC experiments are presented in Text S1 and Figures S1–S3 in Supporting Information S1. Note that after the high P-T measurements, using energy-dispersive X-ray spectroscopy we confirmed the composition of recovered samples remains essentially the same with a slight variation of <1–2 at%.

2.2. Thermal Conductivity Measurements

We coupled time-domain thermoreflectance (TDTR) with LHDAC to precisely measure the thermal conductivity of solid pure Fe and $Fe_{0.85}Ni_{0.06}Si_{0.09}$ at variable high P-T conditions up to ~155 GPa/3246 K and ~148 GPa/2950 K, respectively, with a typical temperature uncertainty of ~150 K (Supplementary Materials). In brief, in our TDTR system, we split the output of a Ti:sapphire laser into pump and probe beams. (The laser's central wavelength was set at 785 nm, under which the Al film coated on the sample has large thermoreflectance signal.) The pump beam, electro-optically modulated at 8.7 MHz, passed through a mechanically-moving stage that changed the pump beam's travel distance to the sample, and eventually heated up the Al film coated on the sample, changing its optical reflectivity. The probe beam then detected the temporal variations in Al's reflectivity, which is associated with the sample's thermal conductivity via thermoreflectance. Details of the TDTR principle along with the analyses of data and uncertainty under high P-T conditions were discussed in Cahill (2004), Chien et al. (2024), Hsieh, Ishii, et al. (2025), Hsieh et al. (2009, 2022) and references therein.

Figures S4 and S5 in Supporting Information S1 illustrate representative TDTR spectra for $Fe_{0.85}Ni_{0.06}Si_{0.09}$ at 100.5 GPa/300 K and 95 GPa/2221 K, respectively, compared with calculations of a bi-directional thermal model that enable the derivation of its thermal conductivity. In our data analysis, the most critical parameters affecting the derived thermal conductivity of the sample are the thickness of Al film and the heat capacity of sample. The thickness of Al under an experimental high P-T condition was estimated following our recently developed method detailed in Hsieh, Chang, et al. (2024) and Hsieh, Ishii, et al. (2025). The heat capacity of pure Fe at high P-T conditions was taken from Hsieh et al. (2020); because the heat capacity of $Fe_{0.85}Ni_{0.06}Si_{0.09}$ at high P-T conditions is not known, we assumed it is similar to that of the $Fe_{0.85}Si_{0.15}$ (Hsieh et al., 2020). This assumption is based on the fact that several properties of Fe and Ni are quite similar to each other, including atomic weight and radius, melting point, thermal conductivity, and most importantly specific heat. Consequently, the replacement of Fe with 7 wt% Ni is expected to have minor effects on the heat capacity, that is, the heat capacity of Fe–7wt%Ni–5wt%Si ($Fe_{0.85}Ni_{0.06}Si_{0.09}$) should be similar to that of Fe–8wt%Si ($Fe_{0.85}Si_{0.15}$), where the effect of 3 wt% difference in Si is expected to be minor. We emphasize that the uncertainty of sample's thermal conductivity is primarily resulted from data analysis (i.e., the uncertainties propagated by the thermal model parameters), not from the measurements, since the raw data are of high quality and precise (Figures S4 and S5 in Supporting Information S1). Moreover, as the thermal conductivities of Fe and $Fe_{0.85}Ni_{0.06}Si_{0.09}$ are both weakly dependent on temperature (Results section), their uncertainties caused by the uncertainty in measurement temperature (~150 K) due to, for example, collection and analysis of thermal radiation or temperature gradient over the probed spot on the sample (Text S1 and Figure S3 in Supporting Information S1), are expected to be minor. As we discuss in Figures S6 and S7 in Supporting Information S1 (Cahill & Watanabe, 2004; X. Zheng et al., 2007), we estimate that the thermal conductivity uncertainty is <10% at P < 30 GPa/300 K, ~10–15% at P = 30–100 GPa/300 K, as well as ~15% at P~100–150 GPa/~2000–3000 K.

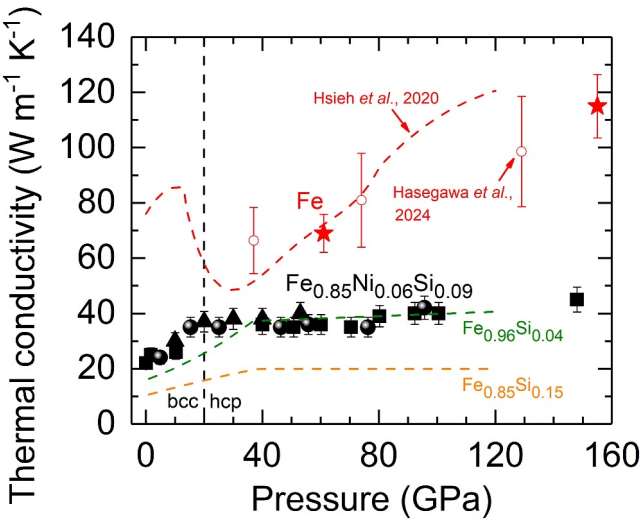

Figure 1. Thermal conductivity of Fe and $Fe_{0.85}Ni_{0.06}Si_{0.09}$ at high pressure and room temperature. The Λ_{Fe} (red stars) is in reasonable agreement with previous results (Hasegawa et al., 2024; Hsieh et al., 2020). As for the $\Lambda_{Fe\text{-}Ni\text{-}Si}$, three individual runs of measurements (each represented by a black symbol shape) show consistent results to ~148 GPa. The error bars indicate uncertainty of data analysis. Literature results for Fe (red dashed line) and binary compositions of $Fe_{0.96}Si_{0.04}$ (green dashed line) and $Fe_{0.85}Si_{0.15}$ (orange dashed line) to ~120 GPa (Hsieh et al., 2020) are plotted for comparison.

3. Results

3.1. High-Pressure, Room-Temperature Thermal Conductivity of Pure Fe and $Fe_{0.85}Ni_{0.06}Si_{0.09}$

Figure 1 presents the pressure dependence of thermal conductivity of pure Fe (Λ_{Fe}) to 155 GPa and $Fe_{0.85}Ni_{0.06}Si_{0.09}$ ($\Lambda_{Fe\text{-}Ni\text{-}Si}$) to 148 GPa at room temperature. The Λ_{Fe} (red stars) is overall in reasonable agreement with literature data (Hasegawa et al., 2024; Hsieh et al., 2020), reaching 115 W m^{-1} K^{-1} at 155 GPa. On the other hand, the combined alloying effect of Ni and Si significantly reduces the $\Lambda_{Fe\text{-}Ni\text{-}Si}$ and alters its pressure dependence as compared to the Fe. $\Lambda_{Fe\text{-}Ni\text{-}Si}$ (black symbols) starts from ~22 W m^{-1} K^{-1}, only ~28% of the Λ_{Fe}, at ambient conditions, and increases with compression until $P \sim 20$ GPa, where a structural transition from body-centered-cubic (bcc) to hexagonal-close-packed (hcp) structure occurs (Morrison et al., 2018). Interestingly, $\Lambda_{Fe\text{-}Ni\text{-}Si}$ in the hcp structure has a fairly weak pressure dependence, saturating to ~40–45 W m^{-1} K^{-1}. This is similar to that of the binary Fe-Si alloys, for example, $Fe_{0.96}Si_{0.04}$ (green dashed line in Figure 1), which also saturates to ~40 W m^{-1} K^{-1}, yet at $P >$ ~40 GPa (Hsieh et al., 2020).

3.2. Thermal Conductivity of Pure Fe and $Fe_{0.85}Ni_{0.06}Si_{0.09}$ at Simultaneously High Pressure-Temperature Conditions

We further combined TDTR with LHDAC to measure the Λ_{Fe} and $\Lambda_{Fe\text{-}Ni\text{-}Si}$ at simultaneously high *P-T* conditions, which allows us to better evaluate the Λ_{Fe} and $\Lambda_{Fe\text{-}Ni\text{-}Si}$ under relevant core *P-T* conditions. As presented in Figure 2a for Fe, both sets of measurements show that the Λ_{Fe} has a positive, but fairly weak temperature dependence. The Λ_{Fe} starting at an ambient cold pressure of 61 GPa (black circles) increases from 69 W m^{-1} K^{-1} at 300 K to ~90 W m^{-1} K^{-1} at 2051 K, in reasonable agreement with previous results at comparable *P-T* conditions (Hasegawa et al., 2024; Kleinschmidt et al., 2023; Saha et al., 2020), considering the measurement and computational uncertainties. In addition, the Λ_{Fe} starting at 155 GPa and 300 K (red squares) is ~115 W m^{-1} K^{-1} and gently increases with temperature, reaching ~145 W m^{-1} K^{-1} at 3246 K, again, in line with those reported by Hasegawa et al. (2024), Kleinschmidt et al. (2023), and Xu et al. (2018) at similar *P-T* conditions when uncertainties are included. Nevertheless, our two sets of data (61 and 155 GPa) both

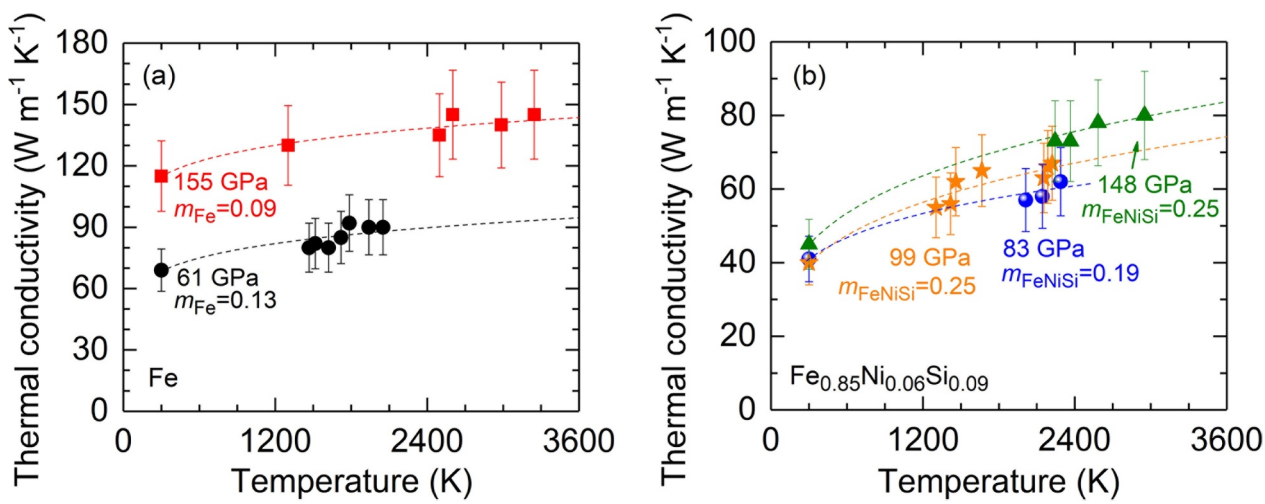

Figure 2. Laser-heated diamond cell measurements on the thermal conductivity of (a) Fe and (b) $Fe_{0.85}Ni_{0.06}Si_{0.09}$ at high pressures and temperatures to ~3246 and ~2950 K, respectively. Both Λ_{Fe} and $\Lambda_{Fe\text{-}Ni\text{-}Si}$ have a positive, yet weak temperature dependence. By modeling the Λ_{Fe} and $\Lambda_{Fe\text{-}Ni\text{-}Si}$ that were assumed to scale with T^m, $m_{Fe} = 0.09$ for Fe at $P \sim 155$ GPa and $T = 300$–3246 K (red squares), while $m_{FeNiSi} = 0.25$ for $Fe_{0.85}Ni_{0.06}Si_{0.09}$ at $P \sim 148$ GPa and $T = 300$–2950 K (green triangles). Dashed curves are fit to each data set for their respective temperature dependence.

report values of $\wedge_{Fe}$ larger than those measured by Konôpková et al. (2016), who showed that $\wedge_{Fe}$ ranges from ~20 to ~45 W m^{-1} K^{-1} at comparable *P-T* conditions.

Ikuta et al. (2021) recently found that the presence of Ni and Si alters the high *P-T* phase stability field of $Fe_{0.85}Ni_{0.06}Si_{0.09}$: at P = 40–160 GPa the $Fe_{0.85}Ni_{0.06}Si_{0.09}$ is in hcp structure between 300 and ~2400 K, while a two-phase mixture of B2 (an ordered derivative of bcc structure) and hcp structure appears at $T >$ ~2400 K. Our present experiments further indicate that the combined alloying effect of Ni and Si also substantially decreases the thermal conductivity at high temperatures, see Figure 2b. Interestingly, three sets of measurements show consistent results with a temperature slope larger than the $\wedge_{Fe}$ within the *P-T* conditions we studied. At a cold pressure of 83 GPa (blue spheres), $\wedge_{Fe\text{-}Ni\text{-}Si}$ increases from ~41 W m^{-1} K^{-1} at 300 K to ~62 W m^{-1} K^{-1} at 2288 K; starting at 99 GPa (orange stars) $\wedge_{Fe\text{-}Ni\text{-}Si}$ is ~40 W m^{-1} K^{-1} at 300 K and reaches ~67 W m^{-1} K^{-1} at 2221 K. Importantly, at a cold pressure of 148 GPa (green triangles), $\wedge_{Fe\text{-}Ni\text{-}Si}$ starts from ~45 W m^{-1} K^{-1} at 300 K and raises to ~80 W m^{-1} K^{-1} at 2950 K, representing a direct measurement on the thermal conductivity of a representative core composition based on $Fe_{0.85}Ni_{0.06}Si_{0.09}$ at high *P-T* conditions close to Earth's core. We did not observe an abrupt, significant change in $\wedge_{Fe\text{-}Ni\text{-}Si}$ across the potential hcp–two-phase mixture transition at ~2400 K.

We now further derive the temperature dependence of $\wedge_{Fe}$ and $\wedge_{Fe\text{-}Ni\text{-}Si}$ at high *P-T* conditions by assuming that $\Lambda(T)$ can be empirically modeled as $\Lambda(T) = \Lambda_0 T^m$, where Λ_0 is a referenced thermal conductivity at a certain temperature and the m value is obtained by linearly fitting the lnΛ-ln$T$ plot. We find that for $\wedge_{Fe}$, m_{Fe} = 0.13 (±0.03) at 61 GPa and m_{Fe} = 0.09(±0.01) at 155 GPa (Figure 2a), while for $\wedge_{Fe\text{-}Ni\text{-}Si}$, m_{FeNiSi} = 0.19 (±0.02) at 83 GPa and m_{FeNiSi} = 0.25(±0.03) at 99 GPa (Figure 2b). For $\wedge_{Fe\text{-}Ni\text{-}Si}$ at 148 GPa, again, since $\wedge_{Fe\text{-}Ni\text{-}Si}$ does not abruptly change across the potential phase transition at ~2400 K, we assume the appearance of B2 phase has minor effects, thereby obtaining m_{FeNiSi} = 0.25(±0.01) at 148 GPa. These temperature dependences are critical for modeling the $\wedge_{Fe}$ and $\wedge_{Fe\text{-}Ni\text{-}Si}$ at core *P-T* conditions, see Discussions below.

The thermal conductivity of a metal is primarily contributed by its electronic component (Λ_e) and described by WF law via $\Lambda_e = L \times T/\rho$, where L is the Lorenz number, T the absolute temperature, and ρ the electrical resistivity, for example, (Hsieh, Lin, et al., 2024; X. Zheng et al., 2007; Q. Zheng et al., 2017) and references therein. As the experimental temperature is comparable or higher than its Debye temperature, the metal's ρ can be approximated as $\rho_0 + \alpha + \beta T$, where ρ_0 is the residual resistivity due to scattering with impurities, α a temperature-induced resistivity shift, and β a temperature coefficient (W. Williams, 1998; Q. Zheng et al., 2017), that is, $\Lambda_e \sim L \times T/(\rho_0 + \alpha + \beta T)$. Because our measurement temperature range (from 300 to ~3000 K) is comparable or higher than the Debye temperature of Fe and $Fe_{0.85}Ni_{0.06}Si_{0.09}$ (~420 K) (Ashcroft & Mermin, 1976), the impurities of Ni and Si (particularly Si) enhance the residual resistivity and make the term $(\rho_0 + \alpha)$ larger than βT (Hsieh, Deschamps, et al., 2024; Q. Zheng et al., 2017), resulting in an increasing Λ_e of $Fe_{0.85}Ni_{0.06}Si_{0.09}$ with increasing temperature as well as a temperature dependence larger than that of the pure Fe. Similar effects that the impurity enhances the temperature dependence of Λ_e has been observed in Fe-S alloys (Hsieh, Deschamps, et al., 2024).

4. Discussions and Geophysical Implications

4.1. Modeling the Thermal Conductivity of Fe and $Fe_{0.85}Ni_{0.06}Si_{0.09}$ at Core *P-T* Conditions

Our experimental results (Figures 1 and 2) allow us to better pin down the $\wedge_{Fe}$ and $\wedge_{Fe\text{-}Ni\text{-}Si}$ at Earth's core *P-T* conditions, which, in turn, offer significant insights to the thermal evolution and dynamics of core, energy budget powering geodynamo, as well as the maximum age of inner core. To this end, we first modeled the thermal conductivity of *solid* Fe and $Fe_{0.85}Ni_{0.06}Si_{0.09}$ at *P-T* conditions of the outermost core ($P \sim$ 136 GPa and $T \sim$ 4000 K from Hirose et al. (2013)). As $\wedge_{Fe}$ and $\wedge_{Fe\text{-}Ni\text{-}Si}$ both have a fairly weak pressure dependence at $P >$ 120 GPa (Figure 1), it's expected that the changes in $\wedge_{Fe}$ and $\wedge_{Fe\text{-}Ni\text{-}Si}$ around the outermost core *P-T* conditions are predominantly caused by the temperature effect (assuming that $\Lambda(T)$ follows the T^m scaling that we derived in Figure 2), rather than the pressure effect. Therefore, at the outermost core conditions, $\wedge_{Fe}$ in solid phase is ~152(±22) W m^{-1} K^{-1}, while $\wedge_{Fe\text{-}Ni\text{-}Si}$ in solid phase is ~86(±13) W m^{-1} K^{-1} (the uncertainty includes that from the data analysis and modeling). Each of them, in turn, sets an upper bound for their thermal conductivity in liquid phase relevant to the liquid outer core. Prior studies have suggested that upon melting, the thermal conductivity of solid Fe and Fe alloys are expected to decrease by ~10%–20% (e.g., Hsieh et al., 2020; Konôpková et al., 2016; Ohta et al., 2016; Pozzo et al., 2014; Silber et al., 2018, 2019; Xu et al., 2018). As such, if the Earth's

liquid outer core is majorly composed of $Fe_{0.85}Ni_{0.06}Si_{0.09}$, it has a moderate thermal conductivity of ~73(±11) W m^{-1} K^{-1} at its top region (assuming a 15% reduction upon melting). For comparison, a liquid outer core with pure Fe composition is much more thermally conductive—$\wedge_{Fe}$ ~ 129(±19) W m^{-1} K^{-1} at its top region. This value is in reasonable agreement with those calculated by de Koker et al. (2012) and Pozzo et al. (2012) and indicates a strong compositional effect on the core thermal conductivity when compared to $\wedge_{Fe\text{-}Ni\text{-}Si}$. Given their relatively weak temperature dependence of thermal conductivity, the uncertainty in the modeled values of $\wedge_{Fe}$ and $\wedge_{Fe\text{-}Ni\text{-}Si}$ due to the potential uncertainty in core temperature (adiabat) is essentially negligible. Finally, we note that a larger reduction of thermal conductivity by ~20%–40% upon melting had also been suggested, for example, (Saha & Mukherjee, 2023), which, if correct, will further strengthen our finding—a moderate thermal conductivity of liquid $Fe_{0.85}Ni_{0.06}Si_{0.09}$ at the top of outer core.

4.2. Geophysical Implications on Core Thermal Evolution and Geodynamo

Prior studies have reported a wide range of thermal conductivity at the top region of liquid core, ~20–250 W m^{-1} K^{-1}, where the large uncertainty is presumably due to the reliability of distinct experimental and computational methods as well as the different, yet uncertain effects of light elements (e.g., Berrada & Secco, 2021; Hsieh et al., 2020; Landeau et al., 2022; Pozzo et al., 2022 and references therein). The moderate thermal conductivity, ~73(±11) W m^{-1} K^{-1}, that we constrain for a liquid core with $Fe_{0.85}Ni_{0.06}Si_{0.09}$ composition falls within the moderate zone over such a broad spectrum of thermal conductivity, reconciling the controversy on the available energy powering geodynamo over the Earth's history. To sustain a thermally-driven geodynamo, a minimum power required to be extracted from the core is set by the core thermal conductivity. With such a moderate core conductivity of ~73(±11) W m^{-1} K^{-1}, the isentropic core heat flow Q_a, defined as the product of core thermal conductivity and isentropic temperature gradient at the outermost core (~1 K km^{-1} (Greenwood et al., 2021)), is estimated to ~11(±1.6) TW. This lower bound heat flow running thermal convection for geodynamo is smaller than (or comparable to) Q_{CMB}, which is controlled by mantle convection and estimated to ~15 TW at present (Frost et al., 2022), although a broad range of ~5–17 TW has also been proposed (Jaupart et al., 2015).

Importantly, the heterogeneous structures at the base of mantle with regionally distinct thermal conductivity (Guerrero et al., 2024; Hsieh, Chang, et al., 2024; Hsieh, Ishii, et al., 2025; Hsieh et al., 2017, 2018) would result in a laterally regional heterogeneity in Q_{CMB}. Figure 3 illustrates this situation with a snapshot of a model of thermochemical convection in spherical annulus geometry. The setup of this model is similar to that in Guerrero et al. (2024), with differences that here the resolution is higher (2,048 × 256 points) and the temperature dependence of mantle thermal conductivity is assumed to be $T^{-0.2}$, which is close to the lower end temperature dependence reported for mantle minerals (Manthilake et al., 2011) and leads to a Q_{CMB} close to 15 TW. Other model parameters include a density contrast between primordial and regular material fixed to 142 kg m^{-3} (equivalent to a buoyancy ratio of 0.23), and an internal heating rate in primordial material assumed to be 10 times higher than in the rest of mantle and leading to a total internal (radiogenic) heating rate equivalent to 11 TW. This simulation features, in particular, stable piles of dense, hot primordial material (Figure 3b) modeling the large-low-velocity-provinces (LLVPs) observed by seismic tomography. Its average CMB heat flux (Φ_{CMB}) is 93.5 mW m^{-2} (corresponding to a total Q_{CMB} of 14.2 TW), but the local heat flux varies between 1.2 mW m^{-2} (i.e., well below the isentropic core heat flux, Φ_a, of 73 mW m^{-2}, suggested by our estimate of core conductivity) and 365 mW m^{-2} (Figure 3d). More specifically, the Φ_{CMB} falls below Φ_a throughout the piles of dense material, where temperature is much higher than average, suggesting that, in the real Earth, Φ_{CMB} may be substantially lower than the Φ_a under part or most of LLVPs.

In case Φ_{CMB} at a certain region becomes smaller than Φ_a (subadiabatic) during core thermochemical evolution (e.g., under the hot piles interiors), a laterally and regionally heterogeneous thermal stratification layer at the topmost core could be formed (Mound et al., 2019). The thickness of such stratified layer may vary from tens to hundreds of kilometers, depending on the spatiotemporal evolution of Φ_{CMB} and Φ_a (Gomi et al., 2013; Labrosse, 2015; Pozzo et al., 2022). Nevertheless, the global geodynamo can still be active at greater depth, if compositional convection occurs due to the inner core solidification that releases buoyant light elements. Interestingly, very recent 1D numerical modellings by Nakagawa et al. (2025) show that with a present-day Q_{CMB} of ~13–15 TW, a core thermal conductivity of ~77–121 W m^{-1} K^{-1} could lead to an ~50 km-thick stratified layer at the top of core, while a long-term stable magnetic field can coexist since ~4 Ga. Our present findings

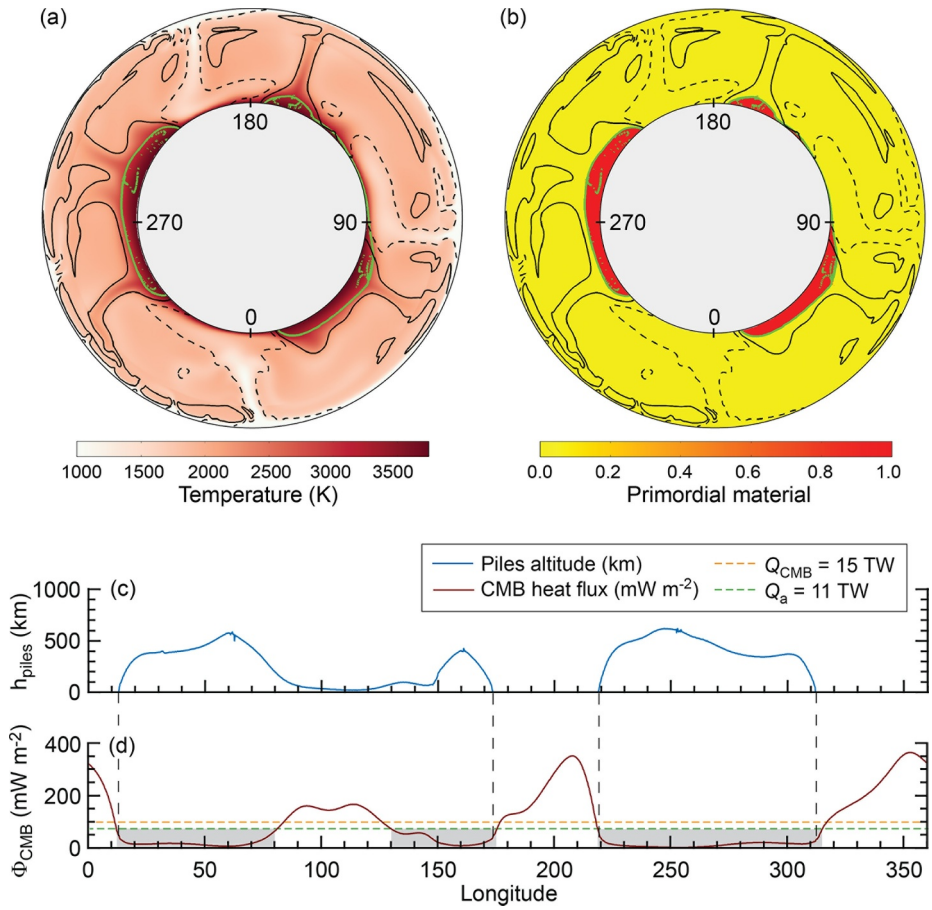

Figure 3. Snapshot of a model of thermochemical convection. (a) Temperature and (b) primordial material fields. (c) Altitude of piles of primordial material, h_{piles}, and (d) core-mantle boundary (CMB) heat flux, Φ_{CMB}, as a function of longitude. In panel (d), the orange dashed line represents the average heat flux for a CMB power of ~15 TW (Frost et al., 2022), and the green dashed line shows the isentropic core heat flux, Φ_a, based on our estimate of the core conductivity. The gray shaded areas indicate regions where $\Phi_{CMB} < \Phi_a$, which mostly correspond to hot piles interiors.

suggest that, unless the present-day Q_{CMB} is overestimated, both the thermal and compositional convections contribute to operate the present geodynamo (Landeau et al., 2022), avoiding the new core paradox (Olson, 2013).

Moreover, based on core thermal evolution model that considers a pure thermally-driven geodynamo before inner core growth and sets Q_{CMB} always equal to Q_a (Gomi et al., 2013; Hsieh et al., 2020; Labrosse, 2015), our moderate core conductivity, ~73(±11) W m^{-1} K^{-1}, would infer a maximum inner core age of ~0.8–1.3 Gyrs (this range could vary slightly with different thermal evolution models and parameter settings). Paleomagnetic studies have reported increases in the geomagnetic field strength at ~0.565 Ga (Bono et al., 2019) and ~1–1.5 Ga (Biggin et al., 2015), often attributed to inner core growth, although more reliable data are required to draw convincing conclusions. Considering the uncertainties in the modellings and experiments, our inferred maximum age of inner core falls in-between and reasonably covers the timing proposed by paleomagnetic studies. Alternatively, it may imply that the composition of liquid core is primarily $Fe_{0.85}Ni_{0.06}Si_{0.09}$ with some amounts of other light elements, for example, O, S, or C, that could slightly change the thermal conductivity and thus the inferred inner core age. Future experimental and computational studies are needed to better quantify the effects of various light elements on Fe-Ni alloy's thermal conductivity. Finally, the modest cooling rate of core implies a minimum initial T_{CMB} of ~4500–5000 K (Gomi et al., 2013; Hsieh et al., 2020; Labrosse, 2015), which would have caused extensive melting of the lowermost mantle in early Earth (Gomi et al., 2013; Labrosse, 2015), supporting the presence of a proposed basal magma ocean at the bottom of mantle (Labrosse et al., 2007).

5. Conclusion

With our high *P-T* LHDAC measurements and data modeling, we have pinned down the thermal conductivity of liquid outer core with $Fe_{0.85}Ni_{0.06}Si_{0.09}$ composition to ~73(±11) W m^{-1} K^{-1} at its top region. Such a moderate value suggests a modest cooling that would allow a long-lived thermal geodynamo and a maximum inner core age of ~0.8–1.3 Gyrs. Though direct high *P-T* measurements are extremely challenging, they are critically required to further quantify the thermal conductivity of liquid phase, or at least the effects of melting, of other elements, for example, O, S, and C. Since the presence of impurities typically suppresses transport of electrical and thermal energy, future studies on Fe-Ni-multiple light elements could further support our present finding of a moderately (or even poorly) thermally conductive core. Future collaborations between experiments and numerical modellings on core thermal evolution and dynamics may then be able to resolve the long-term controversy on the energy budget for geodynamo, and significantly advance our understanding of the complex thermochemical and geomagnetic evolutions over Earth's history.

Conflict of Interest

The authors declare no conflicts of interest relevant to this study.

Data Availability Statement

The data used in this paper are available at (Hsieh, Chiang, et al., 2025) https://doi.org/10.5281/zenodo.17184617.

Acknowledgments
This work was partially supported by the Academia Sinica and the National Science and Technology Council (NSTC) of Taiwan, Republic of China, under Contract AS-IA-111-M02 and NSTC 113-2628-M-001-013 (W.P.H.), AS-IA-113-M02 and NSTC 113-2116-M-001-021 (F.D.), and the JSPS Kakenhi Grant JP24K00722 (E. O.) and JP24K00734 (D.I.).

References

Akahama, Y., & Kawamura, H. (2004). High-pressure Raman spectroscopy of diamond anvils to 250 GPa: Method for pressure determination in the multimegabar pressure range. *Journal of Applied Physics*, *96*(7), 3748–3751. https://doi.org/10.1063/1.1778482

Ashcroft, N. W., & Mermin, N. D. (1976). *Solid state physics*. Thomson Learning, Inc.

Badro, J., Siebert, J., & Nimmo, F. (2016). An early geodynamo driven by exsolution of mantle components from Earth's core. *Nature*, *536*(7616), 326–328. https://doi.org/10.1038/nature18594

Berrada, M., & Secco, R. A. (2021). Review of electrical resistivity measurements and calculations of Fe and Fe-Alloys relating to planetary cores. *Frontiers in Earth Science*, *9*, 732289. https://doi.org/10.3389/feart.2021.732289

Biggin, A. J., Piispa, E. J., Pesonen, L. J., Holme, R., Paterson, G. A., Veikkolainen, T., & Tauxe, L. (2015). Palaeomagnetic field intensity variations suggest Mesoproterozoic inner-core nucleation. *Nature*, *526*(7572), 245–248. https://doi.org/10.1038/nature15523

Bono, R. K., Tarduno, J. A., Nimmo, F., & Cottrell, R. D. (2019). Young inner core inferred from Ediacaran ultra-low geomagnetic field intensity. *Nature Geoscience*, *12*(2), 143–147. https://doi.org/10.1038/s41561-018-0288-0

Cahill, D. G. (2004). Analysis of heat flow in layered structures for time-domain thermoreflectance. *Review of Scientific Instruments*, *75*(12), 5119–5122. https://doi.org/10.1063/1.1819431

Cahill, D. G., & Watanabe, F. (2004). Thermal conductivity of isotopically pure and Ge-doped Si epitaxial layers from 300 to 550 K. *Physical Review B: Condensed Matter and Materials Physics*, *70*(23), 1–3. https://doi.org/10.1103/PhysRevB.70.235322

Chien, Y. H., Marzotto, E., Tsao, Y. C., & Hsieh, W. P. (2024). Anisotropic thermal conductivity of antigorite along slab subduction impacts seismicity of intermediate-depth earthquakes. *Nature Communications*, *15*(1), 5198. https://doi.org/10.1038/s41467-024-49418-3

Cormier, V. F., Bergman, M. I., & Olson, P. L. (2021). *Earth's core: Geophysics of a planet's deepest interior*. Elsevier. https://doi.org/10.1016/C2016-0-01648-0

de Koker, N., Steinle-Neumann, G., & Vlček, V. (2012). Electrical resistivity and thermal conductivity of liquid Fe alloys at high P and T, and heat flux in Earth's core. *Proceedings of the National Academy of Sciences*, *109*(11), 4070–4073. https://doi.org/10.1073/pnas.1111841109

Dobrosavljevic, V. V., Zhang, D., Sturhahn, W., Zhao, J., Toellner, T. S., Chariton, S., et al. (2022). Melting and phase relations of Fe-Ni-Si determined by a multi-technique approach. *Earth and Planetary Science Letters*, *584*, 117358. https://doi.org/10.1016/j.epsl.2021.117358

Frost, D. A., Avery, M. S., Buffett, B. A., Chidester, B. A., Deng, J., Dorfman, S. M., et al. (2022). Multidisciplinary constraints on the thermal-chemical boundary between Earth's core and mantle. *Geochemistry, Geophysics, Geosystems*, *23*(3), e2021GC009764. https://doi.org/10.1029/2021GC009764

Gomi, H., Hirose, K., Akai, H., & Fei, Y. (2016). Electrical resistivity of substitutionally disordered hcp Fe–Si and Fe–Ni alloys: Chemically-induced resistivity saturation in the Earth's core. *Earth and Planetary Science Letters*, *451*, 51–61. https://doi.org/10.1016/j.epsl.2016.07.011

Gomi, H., Ohta, K., Hirose, K., Labrosse, S., Caracas, R., Verstraete, M. J., & Hernlund, J. W. (2013). The high conductivity of iron and thermal evolution of the Earth's core. *Physics of the Earth and Planetary Interiors*, *224*, 88–103. https://doi.org/10.1016/j.pepi.2013.07.010

Greenwood, S., Davies, C. J., & Mound, J. E. (2021). On the evolution of thermally stratified layers at the top of Earth's core. *Physics of the Earth and Planetary Interiors*, *318*, 106763. https://doi.org/10.1016/j.pepi.2021.106763

Guerrero, J. M., Deschamps, F., Hsieh, W. P., & Tackley, P. J. (2024). The combined effect of heterogeneous thermal conductivity, chemical density contrast, and heat-producing element enrichment on the stability of primordial reservoirs above the core-mantle boundary. *Earth and Planetary Science Letters*, *637*, 118699. https://doi.org/10.1016/j.epsl.2024.118699

Hasegawa, A., Ohta, K., Yagi, T., Hirose, K., & Yamashita, Y. (2024). Inversion of the temperature dependence of thermal conductivity of hcp iron under high pressure. *Scientific Reports*, *14*(1), 23582. https://doi.org/10.1038/s41598-024-74110-3

Hirose, K., Labrosse, S., & Hernlund, J. (2013). Composition and State of the core. *Annual Review of Earth and Planetary Sciences*, *41*(1), 657–691. https://doi.org/10.1146/annurev-earth-050212-124007

Hirose, K., Morard, G., Sinmyo, R., Umemoto, K., Hernlund, J., Helffrich, G., & Labrosse, S. (2017). Crystallization of silicon dioxide and compositional evolution of the Earth's core. *Nature*, *543*(7643), 99–102. https://doi.org/10.1038/nature21367

Hirose, K., Wood, B., & Vočadlo, L. (2021). Light elements in the Earth's core. *Nature Reviews Earth & Environment*, *2*(9), 645–658. https://doi.org/10.1038/s43017-021-00203-6

Hsieh, W.-P., Chang, Y. Y., Tsao, Y. C., Lin, C. H., & Vilella, K. (2024). Exceptionally low thermal conduction of basaltic glasses and implications for the thermo-chemical evolution of the Earth's primitive magma Ocean. *Journal of Geophysical Research: Solid Earth*, *129*(2), e2023JB027722. https://doi.org/10.1029/2023JB027722

Hsieh, W.-P., Chen, B., Li, J., Keblinski, P., & Cahill, D. G. (2009). Pressure tuning of the thermal conductivity of the layered muscovite crystal. *Physical Review B: Condensed Matter and Materials Physics*, *80*(18), 180302. https://doi.org/10.1103/PhysRevB.80.180302

Hsieh, W.-P., Chiang, Y.-T., Deschamps, F., Chen, C.-C., Chang, J.-W., Ikuta, D., & Ohtani, E. (2025). Thermal conductivity of Fe and FeNiSi alloy at high pressure and temperature conditions [Dataset]. *Zenodo*. https://doi.org/10.5281/zenodo.17184617

Hsieh, W.-P., Deschamps, F., Okuchi, T., & Lin, J.-F. (2017). Reduced lattice thermal conductivity of Fe-bearing bridgmanite in Earth's deep mantle. *Journal of Geophysical Research: Solid Earth*, *122*(7), 4900–4917. https://doi.org/10.1002/2017jb014339

Hsieh, W.-P., Deschamps, F., Okuchi, T., & Lin, J. F. (2018). Effects of iron on the lattice thermal conductivity of Earth's deep mantle and implications for mantle dynamics. *Proceedings of the National Academy of Sciences of the United States of America*, *115*(16), 4099–4104. https://doi.org/10.1073/pnas.1718557115

Hsieh, W.-P., Deschamps, F., Tsao, Y.-C., Yoshino, T., & Lin, J.-F. (2024). A thermally conductive Martian core and implications for its dynamo cessation. *Science Advances*, *10*(12), eadk1087. https://doi.org/10.1126/sciadv.adk1087

Hsieh, W.-P., Goncharov, A. F., Labrosse, S., Holtgrewe, N., Lobanov, S. S., Chuvashova, I., et al. (2020). Low thermal conductivity of iron-silicon alloys at Earth's core conditions with implications for the geodynamo. *Nature Communications*, *11*(1), 3332. https://doi.org/10.1038/s41467-020-17106-7

Hsieh, W.-P., Ishii, T., Deschamps, F., Tsao, Y. C., Chang, J. W., & Criniti, G. (2025). Reduced thermal conductivity of hydrous Aluminous Silica and Calcium ferrite-type phase promote water transportation to earth's deep mantle. *Journal of Geophysical Research: Solid Earth*, *130*(1), e2024JB030704. https://doi.org/10.1029/2024JB030704

Hsieh, W.-P., Lin, C. H., Chen, C. C., & Chang, J. W. (2024). Testing the validity of the Wiedemann-Franz law for metals and alloys at high pressures. *Applied Physics Letters*, *125*(25), 252201. https://doi.org/10.1063/5.0234126

Hsieh, W.-P., Marzotto, E., Ishii, T., Dubrovinsky, L., Aslandukova, A. A., Criniti, G., et al. (2022). Low thermal conductivity of hydrous phase D leads to a self-preservation effect within a subducting slab. *Journal of Geophysical Research: Solid Earth*, *127*(6), e2022JB024556. https://doi.org/10.1029/2022JB024556

Ikuta, D., Ohtani, E., & Hirao, N. (2021). Two-phase mixture of iron–nickel–silicon alloys in the Earth's inner core. *Communications Earth & Environment*, *2*(1), 225. https://doi.org/10.1038/s43247-021-00298-1

Jaupart, C., Labrosse, S., Lucazeau, F., & Mareschal, J. C. (2015). Temperatures, heat, and energy in the mantle of the Earth. In *Treatise on geophysics* (2nd ed., pp. 223–270). Elsevier Inc. https://doi.org/10.1016/B978-0-444-53802-4.00126-3

Kleinschmidt, U., French, M., Steinle-Neumann, G., & Redmer, R. (2023). Electrical and thermal conductivity of FCC and hcp iron under conditions of the Earth's core from ab initio simulations. *Physical Review B*, *107*(8), 085145. https://doi.org/10.1103/PhysRevB.107.085145

Konôpková, Z., McWilliams, R. S., Gómez-Pérez, N., & Goncharov, A. F. (2016). Direct measurement of thermal conductivity in solid iron at planetary core conditions. *Nature*, *534*(7605), 99–101. https://doi.org/10.1038/nature18009

Labrosse, S. (2003). Thermal and magnetic evolution of the Earth's core. *Physics of the Earth and Planetary Interiors*, *140*(1–3), 127–143. https://doi.org/10.1016/j.pepi.2003.07.006

Labrosse, S. (2015). Thermal evolution of the core with a high thermal conductivity. *Physics of the Earth and Planetary Interiors*, *247*, 36–55. https://doi.org/10.1016/j.pepi.2015.02.002

Labrosse, S., Hernlund, J. W., & Coltice, N. (2007). A crystallizing dense magma ocean at the base of the Earth's mantle. *Nature*, *450*(7171), 866–869. https://doi.org/10.1038/nature06355

Landeau, M., Fournier, A., Nataf, H. C., Cébron, D., & Schaeffer, N. (2022). Sustaining Earth's magnetic dynamo. *Nature Reviews Earth & Environment*, *3*(4), 255–269. https://doi.org/10.1038/s43017-022-00264-1

Lay, T., Hernlund, J., & Buffett, B. (2008). Core mantle boundary heat flow. *Nature Geoscience*, *1*, 25–32. https://doi.org/10.1038/ngeo.2007.44

Li, J., & Fei, Y. (2003). Experimental constraints on core composition. *Treatise on Geochemistry*, *2*, 568. https://doi.org/10.1016/j.epsl.2014.01.004

Manthilake, G. M., de Koker, N., Frost, D. J., & McCammon, C. A. (2011). Lattice thermal conductivity of lower mantle minerals and heat flux from Earth's core. *Proceedings of the National Academy of Sciences of the United States of America*, *108*(44), 17901–17904. https://doi.org/10.1073/pnas.1110594108

Morrison, R. A., Jackson, J. M., Sturhahn, W., Zhang, D., & Greenberg, E. (2018). Equations of State and Anisotropy of Fe-Ni-Si alloys. *Journal of Geophysical Research: Solid Earth*, *123*(6), 4647–4675. https://doi.org/10.1029/2017JB015343

Mound, J., Davies, C., Rost, S., & Aurnou, J. (2019). Regional stratification at the top of Earth's core due to core–mantle boundary heat flux variations. *Nature Geoscience*, *12*(7), 575–580. https://doi.org/10.1038/s41561-019-0381-z

Nakagawa, T., Takehiro, S., & Sasaki, Y. (2025). Effect of thermal conductivity on the simultaneous formation of a stable region at the top of Earth's core and magnetic field generation over four billion years. *Physics of the Earth and Planetary Interiors*, *365*, 107380. https://doi.org/10.1016/j.pepi.2025.107380

Ohta, K., Kuwayama, Y., Hirose, K., Shimizu, K., & Ohishi, Y. (2016). Experimental determination of the electrical resistivity of iron at Earth's core conditions. *Nature*, *534*(7605), 95–98. https://doi.org/10.1038/nature17957

Olson, P. (2013). The new core paradox. *Science*, *342*, 431–432. https://doi.org/10.1126/science.1243477

O'Rourke, J. G., & Stevenson, D. J. (2016). Powering Earth's dynamo with magnesium precipitation from the core. *Nature*, *529*(7586), 387–389. https://doi.org/10.1038/nature16495

Pourovskii, L. V., Mravlje, J., Pozzo, M., & Alfè, D. (2020). Electronic correlations and transport in iron at Earth's core conditions. *Nature Communications*, *11*(1), 4105. https://doi.org/10.1038/s41467-020-18003-9

Pozzo, M., Davies, C., Gubbins, D., & Alfe, D. (2012). Thermal and electrical conductivity of iron at Earth's core conditions. *Nature*, *485*(7398), 355–358. https://doi.org/10.1038/nature11031

Pozzo, M., Davies, C., Gubbins, D., & Alfè, D. (2014). Thermal and electrical conductivity of solid iron and iron-silicon mixtures at Earth's core conditions. *Earth and Planetary Science Letters*, *393*, 159–164. https://doi.org/10.1016/j.epsl.2014.02.047

Pozzo, M., Davies, C. J., & Alfè, D. (2022). Towards reconciling experimental and computational determinations of Earth's core thermal conductivity. *Earth and Planetary Science Letters*, *584*, 117466. https://doi.org/10.1016/j.epsl.2022.117466

Saha, P., Mazumder, A., & Mukherjee, G. D. (2020). Thermal conductivity of dense hcp iron: Direct measurements using laser heated diamond anvil cell. *Geoscience Frontiers*, *11*(5), 1755–1761. https://doi.org/10.1016/j.gsf.2019.12.010

Saha, P., & Mukherjee, G. D. (2023). Thermal conductivity of iron and nickel during melting: Implication to the planetary liquid outer core. *Pramana - Journal of Physics*, *97*(1), 1. https://doi.org/10.1007/s12043-022-02471-3

Seagle, C. T., Cottrell, E., Fei, Y., Hummer, D. R., & Prakapenka, V. B. (2013). Electrical and thermal transport properties of iron and iron-silicon alloy at high pressure. *Geophysical Research Letters*, *40*(20), 5377–5381. https://doi.org/10.1002/2013GL057930

Shen, G., Wang, Y., Dewaele, A., Wu, C., Fratanduono, D. E., Eggert, J., et al. (2020). Toward an international practical pressure scale: A proposal for an IPPS ruby gauge (IPPS-Ruby2020). *High Pressure Research*, *40*(3), 299–314. https://doi.org/10.1080/08957959.2020.1791107

Silber, R. E., Secco, R. A., Yong, W., & Littleton, J. A. H. (2019). Heat flow in Earth's core from invariant electrical resistivity of Fe-Si on the melting boundary to 9 GPa: Do light elements matter? *Journal of Geophysical Research: Solid Earth*, *124*(6), 5521–5543. https://doi.org/10.1029/2019JB017375

Silber, R. E., Secco, R. A., Yong, W., & Littleton, J. A. H. (2018). Electrical resistivity of liquid Fe to 12 GPa: Implications for heat flow in cores of terrestrial bodies. *Scientific Reports*, *8*(1), 10758. https://doi.org/10.1038/s41598-018-28921-w

Tarduno, J., Cottrell, R., Davis, W., Nimmo, F., & Bono, R. (2015). A Hadean to Paleoarchean geodynamo recorded by single zircon crystals. *Science*, *349*(6247), 521–524. https://doi.org/10.1126/science.aaa9114

Tarduno, J., Cottrell, R. D., Watkeys, M. K., Hofmann, A., Doubrovine, P. V., Mamajek, E. E., et al. (2010). Geodynamo, solar wind, and magnetopause 3.4 to 3.45 billion years ago. *Science*, *327*(5970), 1238–1240. https://doi.org/10.1126/science.1183445

Williams, Q. (2018). The thermal conductivity of Earth's core: A key geophysical parameter's constraints and uncertainties. *Annual Review of Earth and Planetary Sciences*, *46*(1), 47–66. https://doi.org/10.1146/annurev-earth-082517-010154

Williams, W. (1998). The thermal conductivity of metallic ceramics. *Journal of the Minerals Metals & Materials Society*, *50*(6), 62–66. https://doi.org/10.1007/s11837-998-0131-y

Xu, J., Zhang, P., Haule, K., Minar, J., Wimmer, S., Ebert, H., & Cohen, R. E. (2018). Thermal conductivity and electrical resistivity of solid iron at Earth's core conditions from first principles. *Physical Review Letters*, *121*(9), 096601. https://doi.org/10.1103/PhysRevLett.121.096601

Yin, Y., Wang, L., Zhai, S., & Liu, Y. (2024). Lorenz number and transport properties of Fe: Implications to the thermal conductivity at Earth's core-mantle boundary. *American Mineralogist*, *109*(11), 1850–1860. https://doi.org/10.2138/am-2023-9246

Zhang, J. S., Bass, J. D., & Zhu, G. (2015). Single-crystal Brillouin spectroscopy with CO_2 laser heating and variable q. *Review of Scientific Instruments*, *86*(6), 063905. https://doi.org/10.1063/1.4922634

Zhang, Y., Hou, M., Liu, G., Zhang, C., Prakapenka, V. B., Greenberg, E., et al. (2020). Reconciliation of experiments and theory on transport properties of iron and the geodynamo. *Physical Review Letters*, *125*(7), 078501. https://doi.org/10.1103/PhysRevLett.125.078501

Zhang, Y., Luo, K., Hou, M., Driscoll, P., Salke, N. P., Ar, M., et al. (2022). Thermal conductivity of Fe-Si alloys and thermal stratification in Earth's core. *Proceedings of the National Academy of Sciences, USA*, *119*(1), e2119001119. https://doi.org/10.1073/pnas.2119001119

Zheng, Q., Mei, A. B., Tuteja, M., Sangiovanni, D. G., Hultman, L., Petrov, I., et al. (2017). Phonon and electron contributions to the thermal conductivity of VN_x epitaxial layers. *Physical Review Materials*, *1*(6), 065002. https://doi.org/10.1103/PhysRevMaterials.1.065002

Zheng, X., Cahill, D. G., Krasnochtchekov, P., Averback, R. S., & Zhao, J. C. (2007). High-throughput thermal conductivity measurements of nickel solid solutions and the applicability of the Wiedemann-Franz law. *Acta Materialia*, *55*(15), 5177–5185. https://doi.org/10.1016/j.actamat.2007.05.037

References From the Supporting Information

Meng, Y., Hrubiak, R., Rod, E., Boehler, R., & Shen, G. (2015). New developments in laser-heated diamond anvil cell with in situ synchrotron x-ray diffraction at High Pressure Collaborative Access Team. *Review of Scientific Instruments*, *86*(7), 072201. https://doi.org/10.1063/1.4926895

Rainey, E. S. G., Hernlund, J. W., & Kavner, A. (2013). Temperature distributions in the laser-heated diamond anvil cell from 3-D numerical modeling. *Journal of Applied Physics*, *114*(20), 204905. https://doi.org/10.1063/1.4830274

Shen, G., Rivers, M. L., Wang, Y., & Sutton, S. R. (2001). Laser heated diamond cell system at the advanced photon source for in situ x-ray measurements at high pressure and temperature. *Review of Scientific Instruments*, *72*(2), 1273–1282. https://doi.org/10.1063/1.1343867